

Chiral Skyrmions Interacting with Chiral Flowers

Xichao Zhang,^{1,*} Jing Xia,^{2,*} Oleg A. Tretiakov,³ Motohiko Ezawa,⁴ Guoping Zhao,⁵ Yan Zhou,⁶
Xiaoxi Liu,^{2,†} and Masahito Mochizuki^{1,‡}

¹*Department of Applied Physics, Waseda University, Okubo, Shinjuku-ku, Tokyo 169-8555, Japan*

²*Department of Electrical and Computer Engineering, Shinshu University, 4-17-1 Wakasato, Nagano 380-8553, Japan*

³*School of Physics, The University of New South Wales, Sydney 2052, Australia*

⁴*Department of Applied Physics, The University of Tokyo, 7-3-1 Hongo, Tokyo 113-8656, Japan*

⁵*College of Physics and Electronic Engineering, Sichuan Normal University, Chengdu 610068, China*

⁶*School of Science and Engineering, The Chinese University of Hong Kong, Shenzhen, Guangdong 518172, China*

(Dated: December 7, 2023)

ABSTRACT

The chiral nature of active matter plays an important role in the dynamics of active matter interacting with chiral structures. Skyrmions are chiral objects, and their interactions with chiral nanostructures can lead to intriguing phenomena. Here, we explore the random-walk dynamics of a thermally activated chiral skyrmion interacting with a chiral flower-like obstacle in a ferromagnetic layer, which could create topology-dependent outcomes. It is a spontaneous mesoscopic order-from-disorder phenomenon driven by the thermal fluctuations and topological nature of skyrmions that exists only in ferromagnetic and ferromagnetic systems. The interactions between the skyrmions and chiral flowers at finite temperatures can be utilized to control the skyrmion position and distribution without applying any external driving force or temperature gradient. The phenomenon that thermally activated skyrmions are dynamically coupled to chiral flowers may provide a new way to design topological sorting devices.

Keywords: *Skyrmion, chiral flower, topological spin texture, topological sorting, chirality, spintronics*

* X.Z. and J.X. contributed equally to this work.

† Email: liu@cs.shinshu-u.ac.jp

‡ Email: masa_mochizuki@waseda.jp

Chiral skyrmions are versatile topological objects with fixed chirality in magnets with chiral exchange interactions [1–15]. They can be created in magnetic thin films [16, 17], multilayers [18–20], and bulk nanostructures [21–23], where they can also be driven into motion by external forces [3–15]. As skyrmions are usually rigid and nonvolatile [3–15, 24], they could be employed as nanoscale information carriers in next-generation information processing applications [25], including data storage [26, 27] and logic computing [28]. Recent studies also suggest that skyrmions can be used as building blocks in future non-conventional applications, including the neuromorphic [29] and quantum computing [30, 31].

The skyrmion dynamics is essential for skyrmionic devices. The dynamics of chiral skyrmions stabilized by chiral exchange interactions [32, 33] in ferromagnets include two aspects, i.e., the motion driven by applied forces [3–15, 25] and the spontaneous diffusion induced by thermal fluctuations [34–58]. For example, a skyrmion driven by the spin-orbit torques may show the skyrmion Hall effect [39, 42, 59, 60], where the skyrmion moves at an angle with respect to the applied current direction. On the other hand, a skyrmion driven by thermal effects may show the Brownian gyromotion [36–38, 40, 41, 43, 47–50, 56], where the skyrmion tends to move in circular trajectories during the random walk. Skyrmions can also be driven into directional motion by thermal gradients [34, 35, 44, 51]. Both the skyrmion Hall effect and skyrmion Brownian diffusion in the ferromagnetic and ferrimagnetic systems depend on the topological charge carried by the skyrmion (i.e., the skyrmion number), which is defined as $Q = \frac{1}{4\pi} \int \mathbf{m} \cdot (\frac{\partial \mathbf{m}}{\partial x} \times \frac{\partial \mathbf{m}}{\partial y}) dx dy$ with \mathbf{m} being the reduced net magnetization [11]. The topology-dependent dynamic behaviors of skyrmions, either spontaneous or forced, are fundamental for practical applications and require precise control in nanostructures.

An important issue in the control and manipulation of skyrmion dynamics in nanostructures is the skyrmion-substrate interactions [14, 61–65]. In active matter systems, the particle-particle and particle-substrate interactions play an important role in the particle dynamics [66, 67]. As nanoscale skyrmions are usually rigid and can show self-motion at finite temperature (i.e., Brownian motion), they can also be treated as a special type of active quasiparticles and interact with the substrate effectively [14, 24, 61–65, 68]. Moreover, the skyrmion-substrate interactions may result in some unique features due to the nontrivial topological nature of skyrmions [14, 24, 61–65, 68].

In 2013, Mijalkov and Volpe demonstrated the possibility that particle-like chiral microswimmers performing circular active Brownian motion can be sorted in a chiral environment formed by using some static obstacle patterns on the substrate [69, 70], where the chirality of circular

Brownian motion couples to chiral features present in the environment. As skyrmions also show circular Brownian motion due to their nontrivial topology [36–38, 40, 41, 43, 47–50, 56], it is therefore envisioned that the thermally activated random-walk dynamics of skyrmions may also be modified in a chiral environment due to the skyrmion-substrate interactions, which is the focus of this work. However, it should be noted that active matter systems have some form of self-propulsion [66, 67, 69, 70], while the Brownian skyrmions are only undergoing thermal motion and are not self-propelled.

The square and chiral flower-like obstacles considered in this work are schematically depicted in Figure 1. A real example of a chiral flower is given in Figure 1(a), which is a left-handed flower showing a fixed left-contort corolla. The chirality of a flower, either left-handed or right-handed [Figure 1(b)], is an important property of floral symmetry. Some flowers have a contort petal aestivation, which is most pronounced in floral buds and may be less prominent in open flowers [71, 72]. In chiral flowers, two morphs are possible as shown in Figure 1(b): contorted to the left and contorted to the right [71, 72]. Micro- and nanostructures mimicking chiral flowers may control the dynamics of active chiral matter [66, 67, 69, 70] as well as thermally activated chiral skyrmions. In Figure 1(c), a thermally activated skyrmion shows clockwise or counterclockwise Brownian gyromotion, which depends on the sign of Q . If a skyrmion is initially placed within a chiral flower, then it may escape from or be confined by the chiral flower. The outcome depends on the chirality of the flower and the sign of Q , which could result in the topological sorting and create an order (sorting)-from-disorder (Brownian motion) phenomenon. However, if a skyrmion is initially placed within a square obstacle, then it will be confined by the square.

We first show the typical Brownian gyromotion of a ferromagnetic skyrmion within a square obstacle in a two-dimensional model, which results in the confinement of the skyrmion [48, 50, 73]. The length, width, and thickness of the ferromagnetic layer equal 256, 256, and 1 nm, respectively. The square pattern is made of four obstacle bars, which are rectangle regions locally modified to have enhanced PMA K_o . We assume that $K_o/K = 10$ in order to make sure that the skyrmions cannot penetrate the obstacle boundary [74]. Such a square pattern on the ferromagnetic substrate can, in principle, be fabricated in experiments [50, 75–77]. The width of each obstacle bar is 10 nm, and the distance between two parallel inner edges of the square pattern is 100 nm. The distance between the two parallel outer edges is thus 120 nm. The square center overlaps the ferromagnetic layer center, as indicated in Figure 2(a). Other modeling details and parameters are given in Methods.

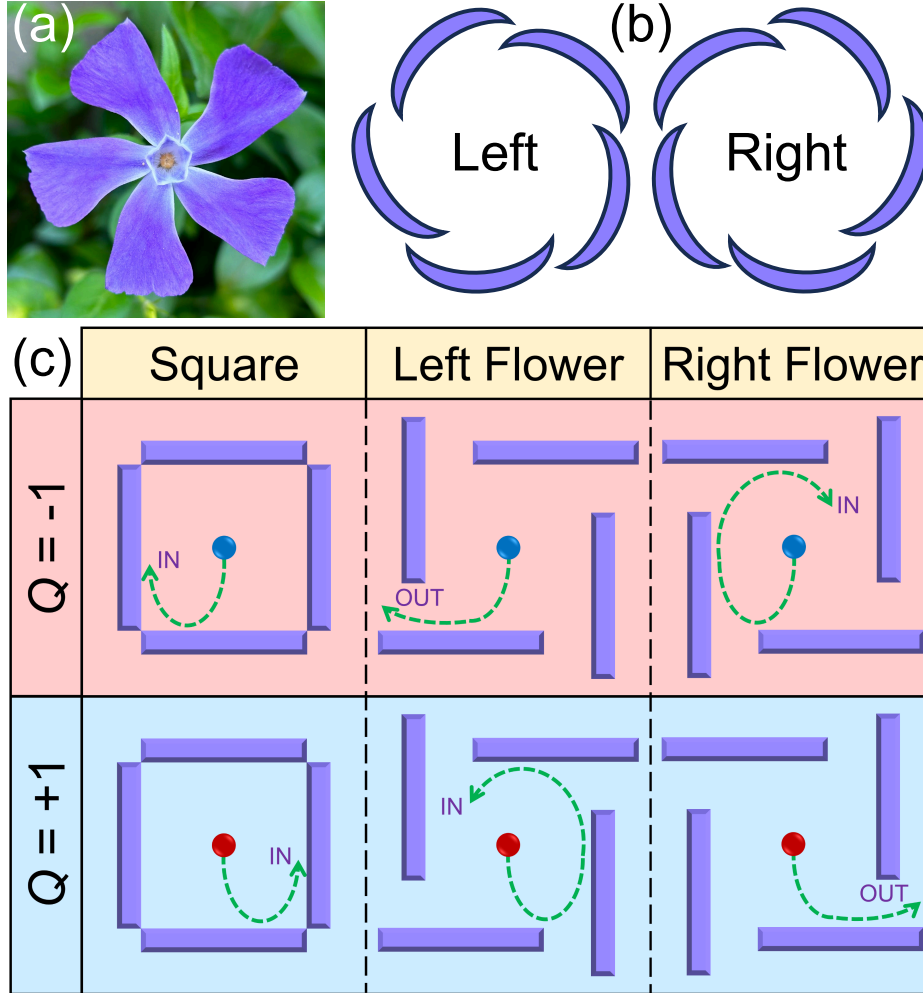


Figure 1. A thermally activated chiral skyrmion interacting with a chiral flower-like obstacle. (a) An exemplary chiral flower (*Vinca minor*) found in Shinjuku City by the authors, which shows a fixed left-contort corolla. (b) Diagrams showing the left-right asymmetry in flowers with fixed corolla contortion, i.e., the left-contort and right-contort corollas. (c) Typical desired outcomes of a chiral skyrmion interacting with a chiral flower or a square: skyrmion confined (i.e., “IN”) and skyrmion escaped (i.e., “OUT”). The outcomes depend on the skyrmion number Q as well as the left-right asymmetry of the chiral flower. The skyrmions with $Q = -1$ and $Q = +1$ are denoted by blue and red dots, respectively.

Initially, a skyrmion is placed and relaxed at the center of the ferromagnetic layer. We then simulate the thermal random-walk dynamics (i.e., the Brownian motion) of the skyrmion at a temperature of $T = 150$ K for 500 ns. The trajectories of the skyrmions with $Q = -1$ and $Q = +1$ are given in Figures 2(a) and 2(b), respectively. The skyrmion with $Q = -1$ shows clockwise Brownian gyromotion [Figure 2(c)] (see Movie S1), while the skyrmion with $Q = +1$ shows

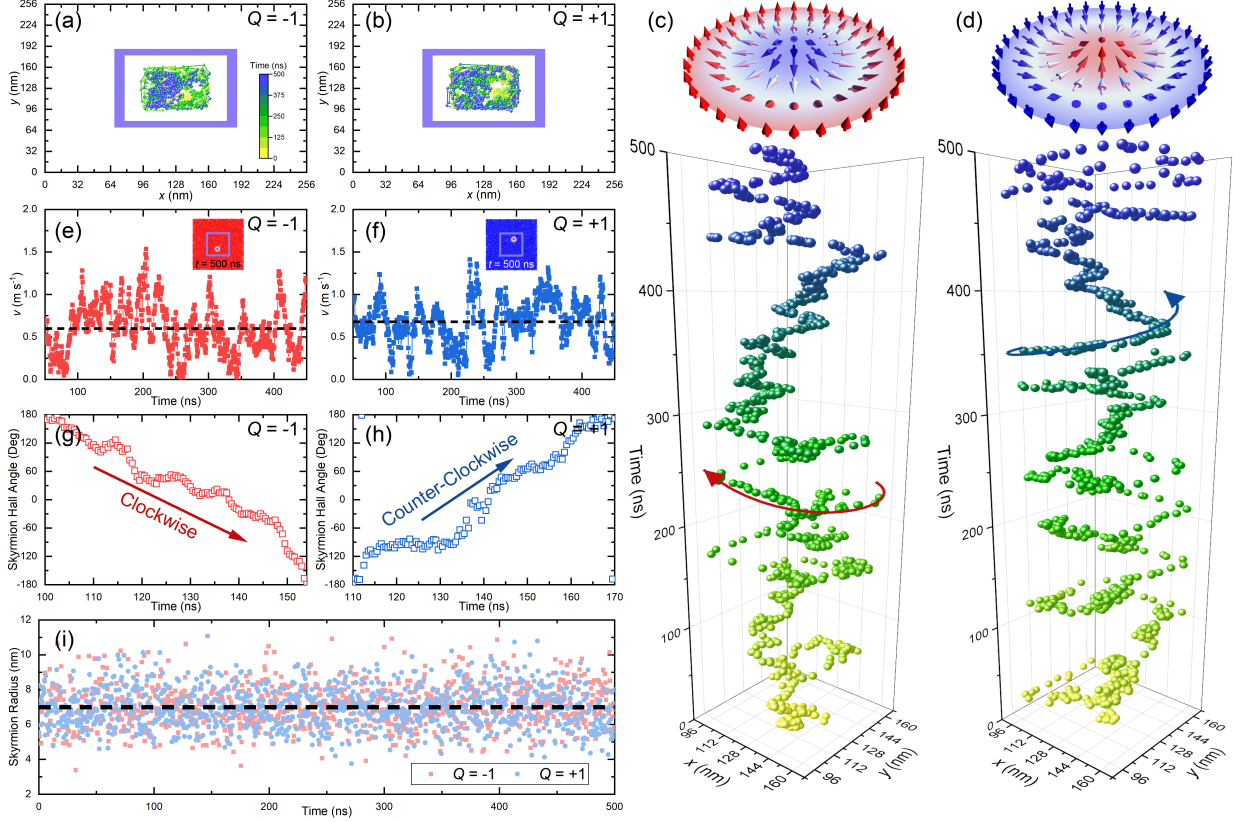


Figure 2. A thermally activated skyrmion confined by a square obstacle. Typical trajectories of (a) a skyrmion with $Q = -1$ and (b) a skyrmion with $Q = +1$ confined by a square are given. Three-dimensional illustrations show the time-dependent skyrmion position and the skyrmion texture with (c) $Q = -1$ or (d) $Q = +1$. The skyrmions with $Q = -1$ and $Q = +1$ show clockwise and counterclockwise circular motion along the inner edges of the square obstacle, respectively. Time-dependent velocities v of the skyrmions with (e) $Q = -1$ and (f) $Q = +1$ are given. Time-dependent skyrmion Hall angles of the skyrmions with (g) $Q = -1$ and (h) $Q = +1$ are also shown for selected time ranges, indicating the clockwise and counterclockwise circular motion, respectively. (i) Time-dependent skyrmion radius. The skyrmion dynamics is simulated at $T = 150$ K for 500 ns with a time step of 0.5 ns. The time step is small enough to show the Brownian motion with a reasonable precision (see Figure S1 in the Supporting Information).

counterclockwise Brownian gyromotion [Figure 2(d)] (see Movie S2). The skyrmions may move along the inner edges of the square and follow the direction of the intrinsic Brownian gyromotion. The confinement leads to a square shape of the overlapped skyrmion position distribution for 500 ns of simulation. The skyrmion motion guided by the square edges is similar to that guided by grain boundaries [47], which may enhance the skyrmion diffusion. The Brownian gyromotion of

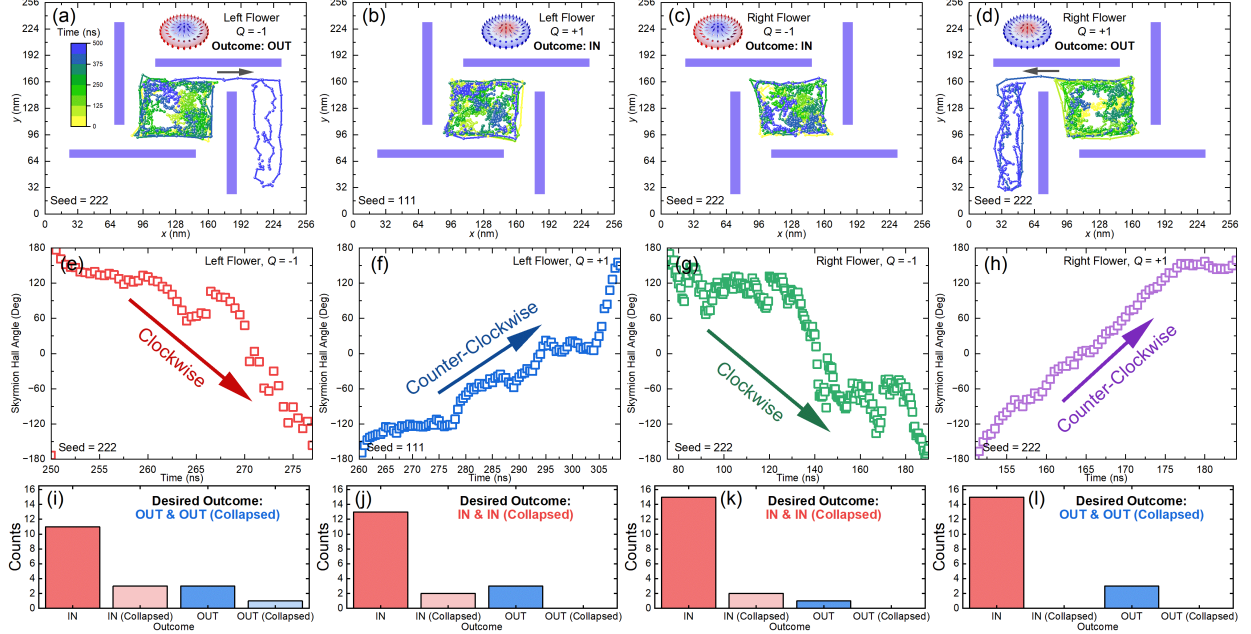


Figure 3. A thermally activated skyrmion interacting with a left-handed or right-handed flower. (a) Typical trajectory of a skyrmion with $Q = -1$ interacting with a left-handed flower. The skyrmion escapes from the left-handed flower due to its clockwise Brownian gyromotion, i.e, the outcome is a desired “OUT”. (b) Typical trajectory of a skyrmion with $Q = +1$ interacting with a left-handed flower. The skyrmion is confined by the left-handed flower due to its counterclockwise Brownian gyromotion, i.e, the outcome is a desired “IN”. (c) Typical trajectory of a skyrmion with $Q = -1$ interacting with a right-handed flower. The skyrmion is confined by the right-handed flower due to its clockwise Brownian gyromotion, i.e, the outcome is a desired “IN”. (d) Typical trajectory of a skyrmion with $Q = +1$ interacting with a right-handed flower. The skyrmion escapes from the right-handed flower due to its counterclockwise Brownian gyromotion, i.e, the outcome is a desired “OUT”. (e)-(h) Time-dependent skyrmion Hall angles for selected time ranges, corresponding to (a) and (b), respectively. (i)-(l) The outcome counts for a skyrmion with $Q = \pm 1$ interacting with a left- or right-handed flower. Eighteen simulations are done with different random seeds for each skyrmion-flower configuration. Both the desired and undesired outcomes are counted. The skyrmion dynamics is simulated at $T = 150$ K for 500 ns with a time step of 0.5 ns.

a skyrmion is a feature of its topological nature, which is due to the Magnus force associated with the net skyrmion number [36–38, 40, 41, 43, 47–50, 56]. We note that the Magnus force is absent in the antiferromagnetic system, where a skyrmion may not show Brownian gyromotion [38, 56].

The time-dependent velocities of the skyrmions with $Q = -1$ and $Q = +1$ interacting with the

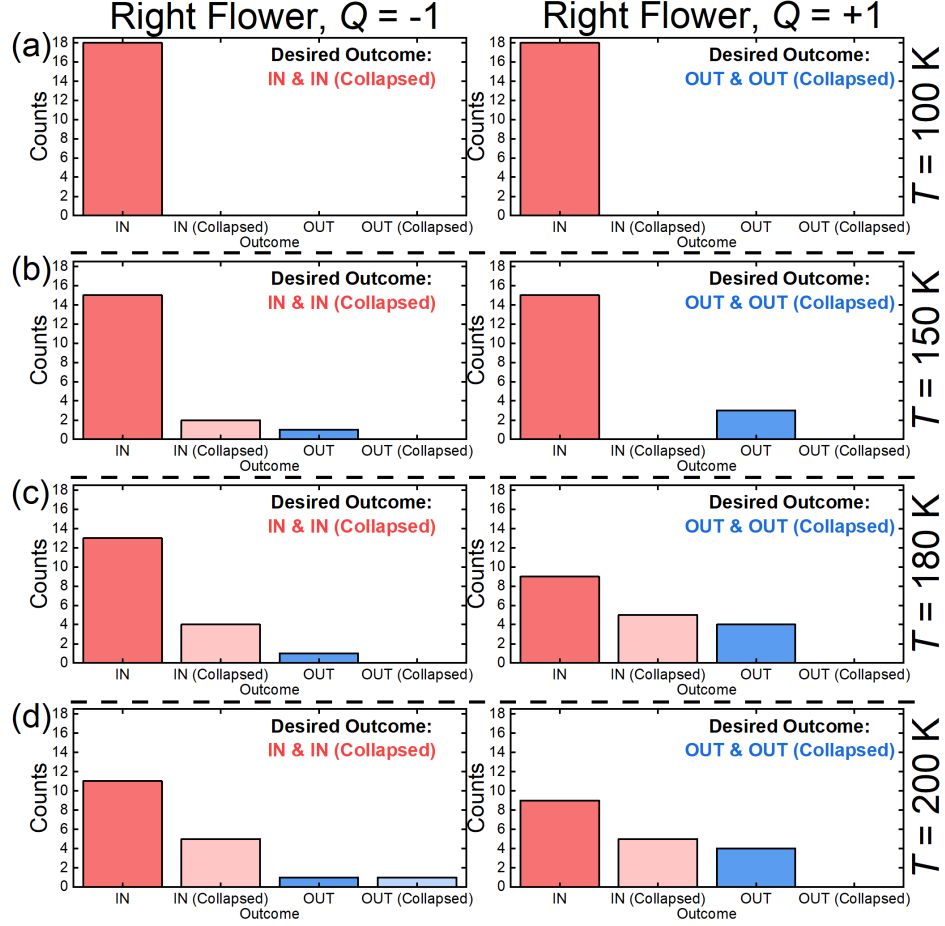


Figure 4. Outcome counts for a skyrmion interacting with a right-handed flower at different temperatures. A skyrmion with $Q = \pm 1$ interacting with a right-handed flower at (a) $T = 100$ K, (b) $T = 150$ K, (c) $T = 180$ K, and (d) $T = 200$ K. Eighteen simulations are done with different random seeds for each temperature. Both desired and undesired outcomes are counted. The skyrmion dynamics is simulated for 500 ns with a time step of 0.5 ns.

square are given in Figure 2(e) and 2(f), respectively. The velocity is randomly fluctuating with time and the mean value for the skyrmion with $Q = -1$ equals 0.60 m s^{-1} , which is almost the same with that of the skyrmion with $Q = -1$ (0.68 m s^{-1}). The clockwise and counterclockwise Brownian gyromotion can also be seen from the time-dependent skyrmion Hall angle defined as $\theta_{\text{SkHE}} = \arctan(v_y/v_x)$ with v_x and v_y being the x and y components of the skyrmion velocity, respectively. In Figure 2(g), the clockwise skyrmion motion is indicated by the continuous decrease and sharp increase of $\theta_{\text{SkHE}}(t)$. The counterclockwise skyrmion motion is indicated by the continuous increase and sharp decrease of $\theta_{\text{SkHE}}(t)$ [Figure 2(h)]. The radius of the skyrmion with

$Q = \pm 1$ interacting with the square is also fluctuating with time, and its mean value equals 7 nm during 500 ns of simulation [Figure 2(i)].

We also demonstrate two typical outcomes of a thermally activated skyrmion with $Q = \pm 1$ interacting with a left- or right-handed flower-like obstacle pattern in a two-dimensional model. The chiral flower pattern is made of four obstacle bars, which are rectangle regions with enhanced PMA $K_o/K = 10$. The width and length of each obstacle bar are equal to 10 and 120 nm, respectively. The distance between the two parallel inner edges of the obstacle bars is 100 nm. The opening width between the two orthogonal obstacle bars is set to 30 nm. The chiral flower center overlaps the ferromagnetic layer center, as shown in Figure 3(a). The opening width should be wider but not much wider than the skyrmion diameter, and the area within the chiral flower should not be too large. Otherwise, the skyrmion may not interact with the chiral flower in an effective way depending on its diffusion at a given temperature. If the opening width is much larger than the skyrmion diameter, the skyrmion should be easier to escape and enter the flower, and travel in all possible directions equally often during long times, leading to achiral results.

A skyrmion is initially placed and relaxed at the ferromagnetic layer center. We then simulate the thermal random-walk dynamics of a skyrmion at a given temperature for 500 ns. We first show typical desired outcomes of the skyrmion with $Q = \pm 1$ interacting with a left- or right-handed flower at $T = 150$ K in Figures 3(a)-3(d). The skyrmion with $Q = -1$ shows the clockwise Brownian gyromotion [Figures 3(e) and 3(g)]. Consequently, its interactions with the left-handed [Figure 3(a)] and right-handed [Figure 3(c)] chiral flowers lead to the desired outcomes “OUT” and “IN”, respectively, within 500 ns of simulation (see Movie S3 and Movie S4). The skyrmions with $Q = +1$ showing the counterclockwise Brownian gyromotion [Figures 3(f) and 3(h)] and interacting with the left-handed [Figure 3(b)] and right-handed [Figure 3(d)] chiral flowers show the desired outcomes “IN” and “OUT”, respectively (see Movie S5 and Movie S6). The desired outcomes for the four skyrmion-flower configurations are summarized schematically in Figure 1(c). The time-dependent velocity and skyrmion radius during the skyrmion-flower interaction are given in Figure S2 (see Supporting Information), and the time-dependent total energy of the system is given in Figure S3 (see Supporting Information).

The desired outcomes may be achieved when the skyrmion interacts effectively with the chiral flower for a long enough time. However, as a skyrmion has a certain lifetime at finite temperature, it may collapse before or after achievement of the desired outcomes. With reasonable computational workload, we carry out 18 simulations with different random seeds for each temperature

and skyrmion-flower configuration and summarize both the desired and undesired outcomes. For the skyrmion with $Q = -1$ interacting with a left-handed flower, we obtain four events of desired outcome in 18 simulations [Figure 3(i)]. For the skyrmion with $Q = +1$ interacting with a left-handed flower, we obtain 15 events of desired outcome [Figure 3(j)], including two cases in which the skyrmion collapses within the chiral flower. We also note that three undesired “OUT” events happen, which may be due to the fact that the skyrmion size is transiently much smaller than the opening width when it moves to an exit of the left-handed flower along the inner edge of the obstacle bar (see Movie S7). Such a situation may be avoided by slightly reducing the opening width or increasing the skyrmion size; however, it also indicates that the skyrmion is able to travel along the path unfavored by the skyrmion-flower interaction, especially during long times or when the skyrmion-flower interaction is ineffective. For the skyrmion with $Q = -1$ interacting with a right-handed flower, we obtain 17 events of the desired outcome [Figure 3(k)]. For the skyrmion with $Q = +1$ interacting with a right-handed flower, we obtain three events of desired outcome [Figure 3(l)]. We note that when the desired outcome is the “IN” event, both effective and ineffective skyrmion-flower interactions may result in the desired outcome. We also show the skyrmion interacting with an achiral square with corner gaps in the Supporting Information (see Figure S4), where it is expected that both skyrmions with $Q = \pm 1$ can escape easily to explore the whole sample, and the outcomes are independent of Q .

In Figure 4, we further show that the counts of achieving the desired and undesired outcomes within the 500 ns-long simulation of the skyrmion-flower interaction depend on the temperature. When the temperature is too low [Figure 4(a); $T = 100$ K], the skyrmion diffusion is weak and it cannot interact with the chiral flower effectively. In such a case, we obtain 18 “IN” events in 18 simulations for the skyrmions with $Q = \pm 1$ within a right-handed flower. When $T = 150$ K [Figure 4(b)], we obtain 17 desired “IN” events for the skyrmion with $Q = -1$ interacting a right-handed flower, and three desired “OUT” events for the skyrmion with $Q = +1$ interacting with a right-handed flower. When $T = 180$ K [Figure 4(c)], we obtain 17 desired “IN” events for the skyrmion with $Q = -1$ interacting a right-handed flower, and four desired “OUT” events for the skyrmion with $Q = +1$ interacting with a right-handed flower. It suggests that the skyrmion-flower interaction could be more effective due to more active skyrmion at elevated temperature. However, when the temperature is too high [Figure 4(d); $T = 200$ K], the thermal fluctuations may result in the collapse of the skyrmion in more simulations due to the significantly reduced skyrmion lifetime. The mean skyrmion size may also increase with the temperature, while the size

and geometry of the chiral flower are fixed. Therefore, the skyrmion may not interact with the chiral flower effectively when the temperature is too high.

In conclusion, we have studied the thermal random-walk dynamics of a ferromagnetic skyrmion in a chiral environment, where the interactions between skyrmions and chiral obstacles (i.e., the chiral flowers) could lead to topology-dependent spontaneous sorting of skyrmions. The position of a skyrmion can be manipulated by using a simple chiral flower-like obstacle pattern at finite temperature in the absence of an external drive if the skyrmion is placed initially at the center of the flower, which is a state of artificially low entropy. Namely, an effective interaction between the chiral flower (either left or right) and the skyrmion (either $Q = -1$ or $+1$) could result in the escape or confinement of the skyrmion. For both outcomes, as the skyrmion tends to explore the whole space (i.e., inside and outside the flower) during long times due to its thermal diffusion, the disorder and entropy of the system should increase with time, while the total energy is conserved over time despite fluctuations due to the thermal effect. Thus, the skyrmion behaviors in such a closed system are in line with the first and second laws of thermodynamics. However, we point out that some systems are more ordered even when there is increased entropy in the ordered state [78].

Our results reveal the unique thermal dynamics of chiral topological spin textures interacting with chiral structures. Our results also suggest that it is possible to build a topological sorting device based on chiral flower-like structures, in which skyrmions with opposite signs of topological charges could generate different dynamic outcomes.

METHODS

Computational Simulations. The simulations are performed by using the micromagnetic simulator MUMAX³ [79, 80] on several commercial graphics processing units, including NVIDIA GeForce RTX 3070 and RTX 3060 Ti. The magnetization dynamics at finite temperature is governed by the stochastic Landau-Lifshitz-Gilbert (LLG) equation [79, 80],

$$\partial_t \mathbf{m} = -\gamma_0 \mathbf{m} \times (\mathbf{h}_{\text{eff}} + \mathbf{h}_f) + \alpha (\mathbf{m} \times \partial_t \mathbf{m}), \quad (1)$$

where $\mathbf{m} = \mathbf{M}/M_S = 1$ is the reduced magnetization, M_S is the saturation magnetization, t is the time, γ_0 is the absolute gyromagnetic ratio, α is the Gilbert damping parameter, $\mathbf{h}_{\text{eff}} = -\frac{1}{\mu_0 M_S} \cdot \frac{\delta \varepsilon}{\delta \mathbf{m}}$ is the effective field with μ_0 and ε being the vacuum permeability constant and average energy

density, respectively. \mathbf{h}_f is a thermal fluctuating field satisfying [79, 80]

$$\begin{aligned} \langle h_i(\mathbf{x}, t) \rangle &= 0, \\ \langle h_i(\mathbf{x}, t) h_j(\mathbf{x}', t') \rangle &= \frac{2\alpha k_B T}{M_S \gamma_0 \mu_0 V} \delta_{ij} \delta(\mathbf{x} - \mathbf{x}') \delta(t - t'), \end{aligned} \quad (2)$$

where i and j are Cartesian components, k_B is the Boltzmann constant, T is the temperature, and V is the volume of a single mesh cell. δ_{ij} and $\delta(\dots)$ denote the Kronecker and Dirac delta symbols, respectively. The energy terms considered in the model include the ferromagnetic exchange energy, interface-induced chiral exchange energy, perpendicular magnetic anisotropy (PMA) energy, and demagnetization energy. Thus, the average energy density is given as [79, 80]

$$\begin{aligned} \varepsilon = & A (\nabla \mathbf{m})^2 + D [m_z (\mathbf{m} \cdot \nabla) - (\nabla \cdot \mathbf{m}) m_z] \\ & - K (\mathbf{n} \cdot \mathbf{m})^2 - \frac{M_S}{2} (\mathbf{m} \cdot \mathbf{B}_d), \end{aligned} \quad (3)$$

where A , D , and K are the ferromagnetic exchange, DM interaction, and PMA constants, respectively. \mathbf{B}_d is the demagnetization field. \mathbf{n} is the unit surface normal vector. m_z is the out-of-plane component of \mathbf{m} . The default magnetic parameters are 26–28, and 74: $\gamma_0 = 2.211 \times 10^5 \text{ m A}^{-1} \text{ s}^{-1}$, $\alpha = 0.1$, $M_S = 580 \text{ kA m}^{-1}$, $A = 15 \text{ pJ m}^{-1}$, $K = 0.8 \text{ MJ m}^{-3}$, and $D = 3 \text{ mJ m}^{-2}$. The mesh size is $2 \times 2 \times 1 \text{ nm}^3$, which ensures good computational accuracy and efficiency. The finite-temperature simulation is performed with a fixed integration time step of 10 fs and a given random seed.

ASSOCIATED CONTENT

Supporting Information

The Supporting Information is available free of charge at [<https://doi.org/10.1021/acs.nanolett.3c03792>].

Additional simulation results, including the time-dependent velocity and radius of a skyrmion interacting with a left or right chiral flower, the time-dependent total energy of the system, the interaction between a skyrmion with a square with corner gaps, and the time-step-dependent skyrmion trajectories. (PDF)

Movie S1: A thermally activated skyrmion with $Q = -1$ interacting with a square obstacle pattern. The skyrmion dynamics is simulated at $T = 150 \text{ K}$ for 500 ns with a time step of 0.5 ns. The

random seed equals 111. It shows the confinement of the skyrmion by the square. In order to show both the skyrmion and obstacle pattern, the movie shows the time-dependent magnetic anisotropy energy density instead of the magnetization. (MP4)

Movie S2: A thermally activated skyrmion with $Q = +1$ interacting with a square obstacle pattern. The skyrmion dynamics is simulated at $T = 150$ K for 500 ns with a time step of 0.5 ns. The random seed equals 111. It shows the confinement of the skyrmion by the square. In order to show both the skyrmion and obstacle pattern, the movie shows the time-dependent magnetic anisotropy energy density instead of the magnetization. (MP4)

Movie S3: A thermally activated skyrmion with $Q = -1$ interacting with a left flower-like obstacle pattern. The skyrmion dynamics is simulated at $T = 150$ K for 500 ns with a time step of 0.5 ns. The random seed equals 222. The skyrmion escapes from the left flower as a desired outcome. In order to show both the skyrmion and obstacle pattern, the movie shows the time-dependent magnetic anisotropy energy density instead of the magnetization. (MP4)

Movie S4: A thermally activated skyrmion with $Q = +1$ interacting with a left flower-like obstacle pattern. The skyrmion dynamics is simulated at $T = 150$ K for 500 ns with a time step of 0.5 ns. The random seed equals 111. The skyrmion is confined by the left flower as a desired outcome. In order to show both the skyrmion and obstacle pattern, the movie shows the time-dependent magnetic anisotropy energy density instead of the magnetization. (MP4)

Movie S5: A thermally activated skyrmion with $Q = -1$ interacting with a right flower-like obstacle pattern. The skyrmion dynamics is simulated at $T = 150$ K for 500 ns with a time step of 0.5 ns. The random seed equals 222. The skyrmion is confined by the right flower as a desired outcome. In order to show both the skyrmion and obstacle pattern, the movie shows the time-dependent magnetic anisotropy energy density instead of the magnetization. (MP4)

Movie S6: A thermally activated skyrmion with $Q = +1$ interacting with a right flower-like obstacle pattern. The skyrmion dynamics is simulated at $T = 150$ K for 500 ns with a time step of 0.5 ns. The random seed equals 222. The skyrmion escapes from the right flower as a desired outcome. In order to show both the skyrmion and obstacle pattern, the movie shows the

time-dependent magnetic anisotropy energy density instead of the magnetization. (MP4)

Movie S7: A thermally activated skyrmion with $Q = +1$ interacting with a left flower-like obstacle pattern. The skyrmion dynamics is simulated at $T = 150$ K for 500 ns with a time step of 0.5 ns. The random seed equals 777. The skyrmion escapes from the left flower as an undesired outcome. In order to show both the skyrmion and obstacle pattern, the movie shows the time-dependent magnetic anisotropy energy density instead of the magnetization. (MP4)

AUTHOR INFORMATION

Corresponding Authors

Xiaoxi Liu; Email: liu@cs.shinshu-u.ac.jp

Masahito Mochizuki; Email: masa_mochizuki@waseda.jp

Complete contact information is available at: [<https://doi.org/10.1021/acs.nanolett.3c03792>].

Author Contributions

X.Z. and J.X. contributed equally to this work. X.Z., M.M. and X.L. conceived the idea. X.L. and M.M. coordinated the project. X.Z. and J.X. performed the computational simulation and the theoretical analysis. X.Z. took a picture of the chiral flower. X.Z. and J.X. drafted the paper and revised it with input from O.A.T., M.E., G.Z., Y.Z., X.L., and M.M. All authors discussed the results and reviewed the paper.

Notes

The authors declare no competing financial interest.

ACKNOWLEDGEMENTS

X.Z. and M.M. acknowledge support by CREST, the Japan Science and Technology Agency (Grant No. JPMJCR20T1). M.M. also acknowledges support by the Grants-in-Aid for Scientific Research from JSPS KAKENHI (Grants No. JP20H00337 and No. JP23H04522), and the Waseda University Grant for Special Research Projects (Grant No. 2023C-140). J.X. was a JSPS International Research Fellow supported by JSPS KAKENHI (Grant No. JP22F22061). O.A.T. acknowledges support by the Australian Research Council (Grant No. DP200101027), the Co-

operative Research Project Program at the Research Institute of Electrical Communication, Tohoku University (Japan), and by the NCMAS grant. M.E. acknowledges support by CREST, JST (Grant No. JPMJCR20T2). G.Z. acknowledges support by the National Natural Science Foundation of China (Grants No. 51771127, No. 51571126, and No. 51772004), and Central Government Funds of Guiding Local Scientific and Technological Development for Sichuan Province (Grant No. 2021ZYD0025). Y.Z. acknowledges support by the National Natural Science Foundation of China (Grants No. 11974298 and No. 12374123), the Shenzhen Fundamental Research Fund (Grant No. JCYJ20210324120213037), the Shenzhen Peacock Group Plan (Grant No. KQTD20180413181702403), and the Guangdong Basic and Applied Basic Research Foundation (Grant No. 2021B1515120047). X.L. acknowledges support by the Grants-in-Aid for Scientific Research from JSPS KAKENHI (Grants No. JP20F20363, No. JP21H01364, No. JP21K18872, and No. JP22F22061).

REFERENCES

- [1] A. N. Bogdanov and D. A. Yablonskii, Thermodynamically stable “vortices” in magnetically ordered crystals: The mixed state of magnets, *Sov. Phys. JETP* **68**, 101 (1989).
- [2] U. K. Röbner, A. N. Bogdanov, and C. Pfleiderer, Spontaneous skyrmion ground states in magnetic metals, *Nature* **442**, 797 (2006).
- [3] N. Nagaosa and Y. Tokura, Topological properties and dynamics of magnetic skyrmions, *Nat. Nanotech.* **8**, 899 (2013).
- [4] M. Mochizuki and S. Seki, Dynamical magnetoelectric phenomena of multiferroic skyrmions, *J. Phys.: Condens. Matter* **27**, 503001 (2015).
- [5] R. Wiesendanger, Nanoscale magnetic skyrmions in metallic films and multilayers: A new twist for spintronics, *Nat. Rev. Mat.* **1**, 16044 (2016).
- [6] G. Finocchio, F. Büttner, R. Tomasello, M. Carpentieri, and M. Kläui, Magnetic skyrmions: From fundamental to applications, *J. Phys. D: Appl. Phys.* **49**, 423001 (2016).
- [7] N. Kanazawa, S. Seki, and Y. Tokura, Noncentrosymmetric magnets hosting magnetic skyrmions, *Adv. Mater.* **29**, 1603227 (2017).
- [8] W. Jiang, G. Chen, K. Liu, J. Zang, S. G. Velthuis, and A. Hoffmann, Skyrmions in magnetic multilayers, *Phys. Rep.* **704**, 1 (2017).
- [9] A. Fert, N. Reyren, and V. Cros, Magnetic skyrmions: Advances in physics and potential applications,

- Nat. Rev. Mater. **2**, 17031 (2017).
- [10] K. Everschor-Sitte, J. Masell, R. M. Reeve, and M. Kläui, Perspective: Magnetic skyrmions-Overview of recent progress in an active research field, J. Appl. Phys. **124**, 240901 (2018).
- [11] X. Zhang, Y. Zhou, K. M. Song, T.-E. Park, J. Xia, M. Ezawa, X. Liu, W. Zhao, G. Zhao, and S. Woo, Skyrmion-electronics: Writing, deleting, reading and processing magnetic skyrmions toward spintronic applications, J. Phys. Condens. Matter **32**, 143001 (2020).
- [12] B. Göbel, I. Mertig, and O. A. Tretiakov, Beyond skyrmions: Review and perspectives of alternative magnetic quasiparticles, Phys. Rep. **895**, 1 (2021).
- [13] C. H. Marrows and K. Zeissler, Perspective on skyrmion spintronics, Appl. Phys. Lett. **119**, 250502 (2021).
- [14] C. Reichhardt, C. J. O. Reichhardt, and M. V. Milosevic, Statics and dynamics of skyrmions interacting with disorder and nanostructures, Rev. Mod. Phys. **94**, 035005 (2022).
- [15] N. Del-Valle, J. Castell-Queralt, L. González-Gómez, and C. Navau, Defect modeling in skyrmionic ferromagnetic systems, APL Mater. **10**, 010702 (2022).
- [16] S. Heinze, K. von Bergmann, M. Menzel, J. Brede, A. Kubetzka, R. Wiesendanger, G. Bihlmayer, and S. Blügel, Spontaneous atomic-scale magnetic skyrmion lattice in two dimensions, Nat. Phys. **7**, 713 (2011).
- [17] N. Romming, C. Hanneken, M. Menzel, J. E. Bickel, B. Wolter, K. von Bergmann, A. Kubetzka, and R. Wiesendanger, Writing and deleting single magnetic skyrmions, Science **341**, 636 (2013).
- [18] W. Jiang, P. Upadhyaya, W. Zhang, G. Yu, M. B. Jungfleisch, F. Y. Fradin, J. E. Pearson, Y. Tserkovnyak, K. L. Wang, O. Heinonen, S. G. E. te Velthuis, and A. Hoffmann, Blowing magnetic skyrmion bubbles, Science **349**, 283 (2015).
- [19] S. Woo, K. Litzius, B. Krüger, M.-Y. Im, L. Caretta, K. Richter, M. Mann, A. Krone, R. M. Reeve, M. Weigand, P. Agrawal, I. Lemesh, M.-A. Mawass, P. Fischer, M. Kläui, and G. S. D. Beach, Observation of room-temperature magnetic skyrmions and their current-driven dynamics in ultrathin metallic ferromagnets, Nat. Mater. **15**, 501 (2016).
- [20] C. Moreau-Luchaire, C. Moutafis, N. Reyren, J. Sampaio, C. A. F. Vaz, N. Van Horne, K. Bouzehouane, K. Garcia, C. Deranlot, P. Warnicke, P. Wohlhüter, J. M. George, M. Weigand, J. Raabe, V. Cros, and A. Fert, Additive interfacial chiral interaction in multilayers for stabilization of small individual skyrmions at room temperature, Nat. Nanotechnol. **11**, 444 (2016).
- [21] S. Mühlbauer, B. Binz, F. Jonietz, C. Pfleiderer, A. Rosch, A. Neubauer, R. Georgii, and P. Böni,

- Skyrmion lattice in a chiral magnet, *Science* **323**, 915 (2009).
- [22] X. Z. Yu, Y. Onose, N. Kanazawa, J. H. Park, J. H. Han, Y. Matsui, N. Nagaosa, and Y. Tokura, Real-space observation of a two-dimensional skyrmion crystal, *Nature* **465**, 901 (2010).
- [23] M. T. Birch, D. Cortés-Ortuño, L. A. Turnbull, M. N. Wilson, F. Groß, N. Träger, A. Laurenson, N. Bukin, S. H. Moody, M. Weigand, G. Schütz, H. Popescu, R. Fan, P. Steadman, J. A. T. Verezhak, G. Balakrishnan, J. C. Loudon, A. C. Twitchett-Harrison, O. Hovorka, H. Fangohr, F. Y. Ogrin, J. Gräfe, and P. D. Hatton, Real-space imaging of confined magnetic skyrmion tubes, *Nat. Commun.* **11**, 1726 (2020).
- [24] S.-Z. Lin, C. Reichhardt, C. D. Batista, and A. Saxena, Particle model for skyrmions in metallic chiral magnets: Dynamics, pinning, and creep, *Phys. Rev. B* **87**, 214419 (2013).
- [25] W. Kang, Y. Huang, X. Zhang, Y. Zhou, and W. Zhao, Skyrmion-Electronics: An overview and outlook, *Proc. IEEE* **104**, 2040 (2016).
- [26] J. Sampaio, V. Cros, S. Rohart, A. Thiaville, and A. Fert, Nucleation, stability and current-induced motion of isolated magnetic skyrmions in nanostructures, *Nat. Nanotechnol.* **8**, 839 (2013).
- [27] R. Tomasello, E. Martinez, R. Zivieri, L. Torres, M. Carpentieri, and G. Finocchio, A strategy for the design of skyrmion racetrack memories, *Sci. Rep.* **4**, 6784 (2014).
- [28] X. Zhang, M. Ezawa, and Y. Zhou, Magnetic skyrmion logic gates: Conversion, duplication and merging of skyrmions, *Sci. Rep.* **5**, 9400 (2015).
- [29] K. M. Song, J.-S. Jeong, B. Pan, X. Zhang, J. Xia, S. Cha, T.-E. Park, K. Kim, S. Finizio, J. Raabe, J. Chang, Y. Zhou, W. Zhao, W. Kang, H. Ju, and S. Woo, Skyrmion-based artificial synapses for neuromorphic computing, *Nat. Electron.* **3**, 148 (2020).
- [30] C. Psaroudaki and C. Panagopoulos, Skyrmion qubits: A new class of quantum logic elements based on nanoscale magnetization, *Phys. Rev. Lett.* **127**, 067201 (2021).
- [31] J. Xia, X. Zhang, X. Liu, Y. Zhou, and M. Ezawa, Universal quantum computation based on nanoscale skyrmion helicity qubits in frustrated magnets, *Phys. Rev. Lett.* **130**, 106701 (2023).
- [32] I. Dzyaloshinskii, A thermodynamic theory of weak ferromagnetism of antiferromagnetics, *J. Phys. Chem. Solids* **4**, 241 (1958).
- [33] T. Moriya, Anisotropic superexchange interaction and weak ferromagnetism, *Phys. Rev.* **120**, 91 (1960).
- [34] L. Kong and J. Zang, Dynamics of an insulating skyrmion under a temperature gradient, *Phys. Rev. Lett.* **111**, 067203 (2013).

- [35] S. Z. Lin, C. D. Batista, C. Reichhardt, and A. Saxena, AC current generation in chiral magnetic insulators and skyrmion motion induced by the spin seebeck effect, *Phys. Rev. Lett.* **112**, 187203 (2014).
- [36] R. E. Troncoso and A. S. Núñez, Brownian motion of massive skyrmions in magnetic thin films, *Ann. Phys.* **351**, 850 (2014).
- [37] C. Schütte, J. Iwasaki, A. Rosch, and N. Nagaosa, Inertia, diffusion, and dynamics of a driven skyrmion, *Phys. Rev. B* **90**, 174434 (2014).
- [38] J. Barker and O. A. Tretiakov, Static and dynamical properties of antiferromagnetic skyrmions in the presence of applied current and temperature, *Phys. Rev. Lett.* **116**, 147203 (2016).
- [39] C. Reichhardt and C. J. O. Reichhardt, Noise fluctuations and drive dependence of the skyrmion Hall effect in disordered systems, *New J. Phys.* **18**, 095005 (2016).
- [40] J. Miltat, S. Rohart, and A. Thiaville, Brownian motion of magnetic domain walls and skyrmions, and their diffusion constants, *Phys. Rev. B* **97**, 214426 (2018).
- [41] T. Nozaki, Y. Jibiki, M. Goto, E. Tamura, T. Nozaki, H. Kubota, A. Fukushima, S. Yuasa, and Y. Suzuki, Brownian motion of skyrmion bubbles and its control by voltage applications, *Appl. Phys. Lett.* **114**, 012402 (2019).
- [42] C. Reichhardt and C. J. O. Reichhardt, Thermal creep and the skyrmion Hall angle in driven skyrmion crystals, *J. Phys.: Condens. Matter* **31**, 07LT01 (2019).
- [43] L. Zhao, Z. Wang, X. Zhang, X. Liang, J. Xia, K. Wu, H. A. Zhou, Y. Dong, G. Yu, K. L. Wang, X. Liu, Y. Zhou, and W. Jiang, Topology-dependent brownian gyromotion of a single skyrmion, *Phys. Rev. Lett.* **125**, 027206 (2020).
- [44] Z. Wang, M. Guo, H. A. Zhou, L. Zhao, T. Xu, R. Tomasello, H. Bai, Y. Dong, S. G. Je, W. Chao, H. S. Han, S. Lee, K. S. Lee, Y. Yao, W. Han, C. Song, H. Wu, M. Carpentieri, G. Finocchio, M. Y. Im, S. Z. Lin, and W. Jiang, Thermal generation, manipulation and thermoelectric detection of skyrmions, *Nat. Electron.* **3**, 672 (2020).
- [45] Y. Yao, X. Chen, W. Kang, Y. Zhang, and W. Zhao, Thermal brownian motion of skyrmion for true random number generation, *IEEE Trans. Electron Devices* **67**, 2553 (2020).
- [46] K. Y. Jing, C. Wang, and X. R. Wang, Random walk of antiferromagnetic skyrmions in granular films, *Phys. Rev. B* **103**, 174430 (2021).
- [47] Y. Zhou, R. Mansell, T. Ala-Nissila, and S. van Dijken, Thermal motion of skyrmion arrays in granular films, *Phys. Rev. B* **104**, 144417 (2021).

- [48] S. Miki, Y. Jibiki, E. Tamura, M. Goto, M. Oogane, J. Cho, R. Ishikawa, H. Nomura, and Y. Suzuki, Brownian motion of magnetic skyrmions in one- and two-dimensional systems, *J. Phys. Soc. Jpn.* **90**, 083601 (2021).
- [49] Y. Suzuki, S. Miki, Y. Imai, and E. Tamura, Diffusion of a magnetic skyrmion in two-dimensional space, *Phys. Lett. A* **413**, 127603 (2021).
- [50] R. Ishikawa, M. Goto, H. Nomura, and Y. Suzuki, Implementation of skyrmion cellular automaton using Brownian motion and magnetic dipole interaction, *Appl. Phys. Lett.* **119**, 072402 (2021).
- [51] X. Yu, F. Kagawa, S. Seki, M. Kubota, J. Masell, F. S. Yasin, K. Nakajima, M. Nakamura, M. Kawasaki, N. Nagaosa, and Y. Tokura, Real-space observations of 60-nm skyrmion dynamics in an insulating magnet under low heat flow, *Nat. Commun.* **12**, 5079 (2021).
- [52] C. Song, N. Kerber, J. Rothörl, Y. Ge, K. Raab, B. Seng, M. A. Brems, F. Dittrich, R. M. Reeve, J. Wang, Q. Liu, P. Virnau, and M. Kläui, Commensurability between element symmetry and the number of skyrmions governing skyrmion diffusion in confined geometries, *Adv. Funct. Mater.* **31**, 2010739 (2021).
- [53] N. Kerber, M. Weißenhofer, K. Raab, K. Litzius, J. Zázvorka, U. Nowak, and M. Kläui, Anisotropic skyrmion diffusion controlled by magnetic-field-induced symmetry breaking, *Phys. Rev. Applied* **15**, 044029 (2021).
- [54] L. Kong, X. Chen, W. Wang, D. Song, and H. Du, Dynamics of interstitial skyrmions in the presence of temperature gradients, *Phys. Rev. B* **104**, 214407 (2021).
- [55] M. Weißenhofer, L. Rózsa, and U. Nowak, Skyrmion dynamics at finite temperatures: Beyond Thiele's equation, *Phys. Rev. Lett.* **127**, 047203 (2021).
- [56] M. Weißenhofer and U. Nowak, Temperature dependence of current-driven and Brownian skyrmion dynamics in ferrimagnets with compensation point, *Phys. Rev. B* **107**, 064423 (2023).
- [57] R. Gruber, M. A. Brems, J. Rothörl, T. Sparmann, M. Schmitt, I. Kononenko, F. Kammerbauer, M.-A. Syskaki, O. Farago, P. Virnau, and M. Kläui, 300-times-increased diffusive skyrmion dynamics and effective pinning reduction by periodic field excitation, *Adv. Mater.* **35**, 2208922 (2023).
- [58] T. Dohi, M. Weißenhofer, N. Kerber, F. Kammerbauer, Y. Ge, K. Raab, J. Zázvorka, M.-A. Syskaki, A. Shahee, M. Ruhwedel, T. Böttcher, P. Pirro, G. Jakob, U. Nowak, and M. Kläui, Enhanced thermally-activated skyrmion diffusion with tunable effective gyrotropic force, *Nat. Commun.* **14**, 5424 (2023).
- [59] W. Jiang, X. Zhang, G. Yu, W. Zhang, X. Wang, M. Benjamin Jungfleisch, J. E. Pearson, X. Cheng, O. Heinonen, K. L. Wang, Y. Zhou, A. Hoffmann, and S. G. E. te Velthuis, Direct observation of the

- skyrmion Hall effect, *Nat. Phys.* **13**, 162 (2017).
- [60] K. Litzius, I. Lemesh, B. Kruger, P. Bassirian, L. Caretta, K. Richter, F. Buttner, K. Sato, O. A. Tretiakov, J. Forster, R. M. Reeve, M. Weigand, I. Bykova, H. Stoll, G. Schutz, G. S. D. Beach, and M. Klaui, Skyrmion Hall effect revealed by direct time-resolved X-ray microscopy, *Nat. Phys.* **13**, 170 (2017).
- [61] C. Reichhardt, D. Ray, and C. J. O. Reichhardt, Quantized transport for a skyrmion moving on a two-dimensional periodic substrate, *Phys. Rev. B* **91**, 104426 (2015).
- [62] C. Reichhardt, D. Ray, and C. J. O. Reichhardt, Magnus-induced ratchet effects for skyrmions interacting with asymmetric substrates, *New J. Phys.* **17**, 073034 (2015).
- [63] C. Reichhardt and C. J. O. Reichhardt, Nonlinear transport, dynamic ordering, and clustering for driven skyrmions on random pinning, *Phys. Rev. B* **99**, 104418 (2019).
- [64] N. P. Vizir, C. Reichhardt, C. J. O. Reichhardt, and P. A. Venegas, Skyrmion dynamics and topological sorting on periodic obstacle arrays, *New J. Phys.* **22**, 053025 (2020).
- [65] X. Zhang, J. Xia, O. A. Tretiakov, M. Ezawa, G. Zhao, Y. Zhou, X. Liu, and M. Mochizuki, Laminar and transiently disordered dynamics of magnetic-skyrmion pipe flow, *Phys. Rev. B* **108**, 144428 (2023).
- [66] C. Bechinger, R. Di Leonardo, H. Löwen, C. Reichhardt, G. Volpe, and G. Volpe, Active particles in complex and crowded environments, *Rev. Mod. Phys.* **88**, 045006 (2016).
- [67] C. J. O. Reichhardt and C. Reichhardt, Ratchet effects in active matter systems, *Annu. Rev. Condens. Matter Phys.* **8**, 51 (2017).
- [68] Z.-Y. Li, D.-Q. Zhang, S.-Z. Lin, W. T. Gozdz, and B. Li, Spontaneous organization and phase separation of skyrmions in chiral active matter, *Soft Matter* **18**, 7348 (2022).
- [69] M. Mijalkov and G. Volpe, Sorting of chiral microswimmers, *Soft Matter* **9**, 6376 (2013).
- [70] G. Volpe, S. Gigan, and G. Volpe, Simulation of the active Brownian motion of a microswimmer, *Am. J. Phys.* **82**, 659 (2014).
- [71] P. K. Endress, Symmetry in flowers: Diversity and evolution, *Int. J. Plant Sci.* **160**, S3 (1999).
- [72] P. K. Endress, Evolution of floral symmetry, *Curr. Opin. Plant Biol.* **4**, 86 (2001).
- [73] A. Monteil, C. B. Muratov, T. M. Simon, and V. V. Slastikov, Magnetic skyrmions under confinement, [arXiv:2208.00058](https://arxiv.org/abs/2208.00058) (2022), Date of access 2023-01-01.
- [74] X. Zhang, J. Xia, and X. Liu, Particle-like skyrmions interacting with a funnel obstacle, *Phys. Rev. B* **106**, 094418 (2022).

- [75] R. Juge, K. Bairagi, K. G. Rana, J. Vogel, M. Sall, D. Maily, V. T. Pham, Q. Zhang, N. Sisodia, M. Foerster, L. Aballe, M. Belmeguenai, Y. Roussigné, S. Auffret, L. D. Buda-Prejbeanu, G. Gaudin, D. Ravelosona, and O. Boulle, Helium ions put magnetic skyrmions on the track, *Nano Lett.* **21**, 2989 (2021).
- [76] K. Ohara, X. Zhang, Y. Chen, Z. Wei, Y. Ma, J. Xia, Y. Zhou, and X. Liu, Confinement and protection of skyrmions by patterns of modified magnetic properties, *Nano Lett.* **21**, 4320 (2021).
- [77] X. Zhang, J. Xia, K. Shirai, H. Fujiwara, O. A. Tretiakov, M. Ezawa, Y. Zhou, and X. Liu, Configurable pixelated skyrmions on nanoscale magnetic grids, *Commun. Phys.* **4**, 255 (2021).
- [78] Y. Geng, G. van Anders, P. M. Dodd, J. Dshemuchadse, and S. C. Glotzer, Engineering entropy for the inverse design of colloidal crystals from hard shapes, *Sci. Adv.* **5**, eaaw0514 (2019).
- [79] A. Vansteenkiste, J. Leliaert, M. Dvornik, M. Helsen, F. Garcia-Sanchez, and B. V. Waeyenberge, The design and verification of MuMax3, *AIP Adv.* **4**, 107133 (2014).
- [80] J. Leliaert, M. Dvornik, J. Mulkers, J. De Clercq, M. V. Milosevic, and B. Van Waeyenberge, Fast micromagnetic simulations on GPU-recent advances made with mumax³, *J. Phys. D: Appl. Phys.* **51**, 123002 (2018).